How to cite: Angew. Chem. Int. Ed. 2024, e202407109
doi.org/10.1002/anie.202407109

Labeling Technologies

An *In-Situ*-Tag-Generation Proximity Labeling Technology for Recording Cellular Interactions

Yunyan Yao, Ru Jia, Chuanming Liu, Haiqi Wang, Ting Li, Xiaocui Zheng, Tong Zhong, Nan Feng, Jiahui Sun, Ke Li, Ran Xie, Lijun Ding, Chao Yan, Lin Ding, and Huangxian Ju*

Abstract: Obtaining information about cellular interactions is fundamental to the elucidation of physiological and pathological processes. Proximity labeling technologies have been widely used to report cellular interactions in situ; however, the reliance on addition of tag molecules typically restricts their application to regions where tags can readily diffuse, while the application in, for example, solid tissues, is susceptible. Here, we propose an "in-situ-tag-generation mechanism" and develop the *GalTag* technology based on galactose oxidase (GAO) for recording cellular interactions within three-dimensional biological solid regions. GAO mounted on bait cells can in situ generate bio-orthogonal aldehyde tags as interaction reporters on prey cells. Using *GalTag*, we monitored the dynamics of cellular interactions and assessed the targeting ability of engineered cells. In particular, we recorded, for the first time, the footprints of Bacillus Calmette-Guérin (BCG) invasion into the bladder tissue of living mice, providing a valuable perspective to elucidate the anti-tumor mechanism of BCG.

[*] Y. Yao, H. Wang, T. Zhong, Dr. N. Feng, J. Sun, K. Li, Prof. L. Ding, Prof. H. Ju
State Key Laboratory of Analytical Chemistry for Life Science, School of Chemistry and Chemical Engineering, Nanjing University, 210023 Nanjing (P. R. China)
E-mail: dinglin@nju.edu.cn

R. Jia, Prof. C. Yan
State Key Laboratory of Pharmaceutical Biotechnology, School of Life Sciences, Nanjing University, 210023 Nanjing (P. R. China)

Dr. C. Liu, Prof. L. Ding
Center for Reproductive Medicine and Obstetrics and Gynecology, Nanjing Drum Tower Hospital, Nanjing University Medical School, 210008 Nanjing (P. R. China)

Dr. C. Liu, Prof. L. Ding
Center for Molecular Reproductive Medicine, Nanjing University, 210008 Nanjing (P. R. China)

T. Li, X. Zheng, Prof. R. Xie
State Key Laboratory of Coordination Chemistry, School of Chemistry and Chemical Engineering, Nanjing University, 210023 Nanjing (P. R. China)

Prof. R. Xie, Prof. C. Yan, Prof. L. Ding
Chemistry and Biomedicine Innovation Center (ChemBIC), Nanjing University, 210023 Nanjing (P. R. China)

Prof. C. Yan
Engineering Research Center of Protein and Peptide Medicine, Ministry of Education, 210023 Nanjing (P. R. China)

Introduction

Probing cell-cell physical interactions in life has become one of the most attractive research hotspots.[1] Proximity labeling technologies are widely used methods for reporting cellular interactions in situ, in which a catalyst is installed on a bait cell to render the attachment of exogenously-added reactive tags to biomolecules adjacent to the interaction site on the prey cell surface in a catalytic fashion, thereby obtaining relevant spatial proximity information (Scheme 1a).[2] Technologies based on this "tag-transfer mechanism" contain two types: contact-independent (the catalyst converts the tags into diffusible radicals that label prey cells within a certain radius)[3] and contact-dependent (the catalyst installs the tags upon contact with prey cells).[4] In the contact-independent strategies, it is possible for several types of radicals that the labeling position may fall outside the interaction area due to radical diffusion. In contrast, the contact-dependent methods depend only on the relative positions of bait and prey cells.

However, all of these tag-transfer technologies require the addition of exogenous reactive tags that serve as substrates. In the presence of biological barriers, the ability of tags to diffuse and accumulate locally in the target region is compromised, thus limiting the use of these proximity labeling methods. For example, cell migration into solid tissues is critical in various biological scenarios (e.g., embryonic development, wound healing, immune response, bacterial invasion and cancer progression), but how to record these interactions in vivo remains largely unresolved.

Hence, there is an urgent need to develop novel cell-cell interaction recording mechanisms that can in situ generate a bio-orthogonal group as a tag at the interaction site (Scheme 1a). The exemption of exogenous tags enables the catalyst-mounted bait cells to "*tag as they go around*" in biological solid regions, providing the "*complete footprint information*" of the interaction process (Scheme 1b); at the same time, the biologically orthogonal groups generated on the prey have a lower steric hindrance.

We identified two requirements for the design of such an "in-situ-tag-generation" recording system: 1) an enzymatic reaction capable of altering the chemical structure of a biomolecular substrate to generate a bio-orthogonal group; 2) a high Michaelis–Menten constant (K_m) to ensure that labeling is driven by cellular interactions;[4a] and a catalytic constant (k_{cat}) fast enough to track rapid interactions.[4a,c,5] Herein, we established *GalTag*, an "in-situ-tag-generation" transcellular proximity labeling technology by exploiting the

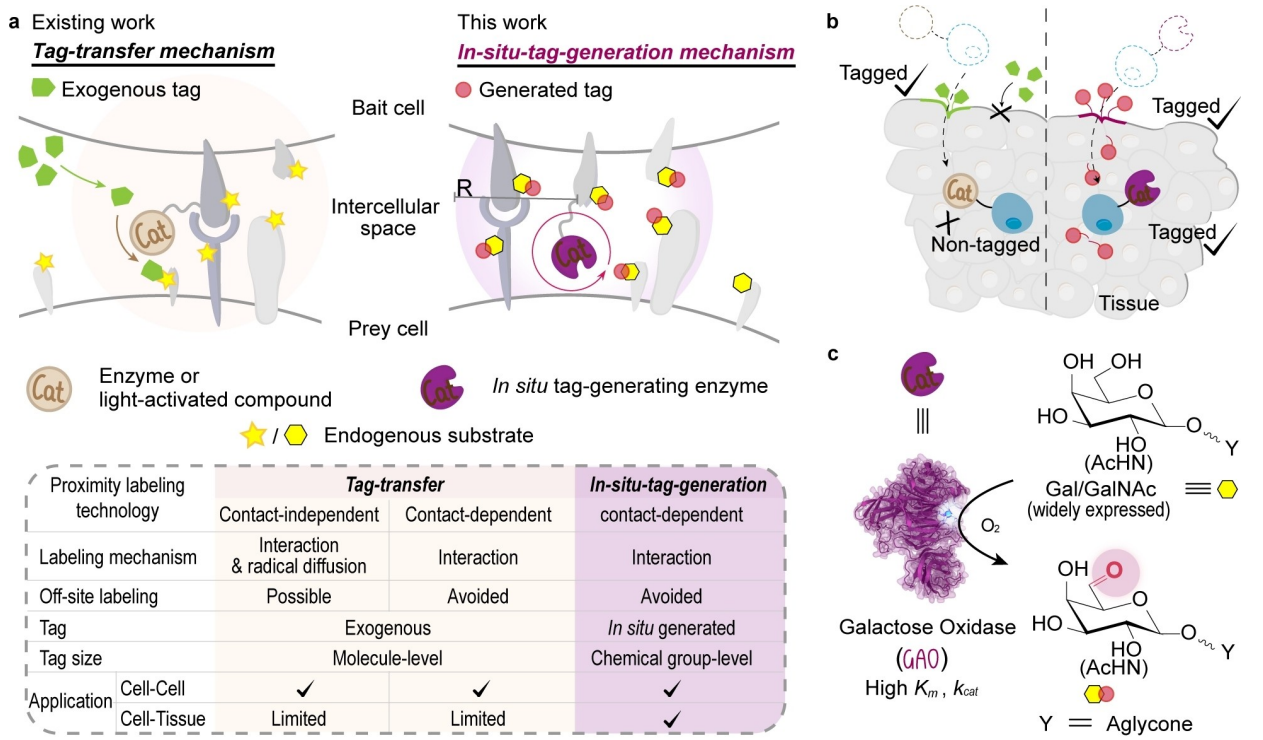

Proximity labeling technology		Tag-transfer		In-situ-tag-generation
		Contact-independent	Contact-dependent	contact-dependent
Labeling mechanism		Interaction & radical diffusion	Interaction	Interaction
Off-site labeling		Possible	Avoided	Avoided
Tag		Exogenous		*In situ* generated
Tag size		Molecule-level		Chemical group-level
Application	Cell-Cell	✓	✓	✓
	Cell-Tissue	Limited	Limited	✓

Scheme 1. Design of the in-situ-tag-generation mechanism and the *GalTag* technology. a, Technology comparison. b, Schematic illustrating the advantage of the in-situ-tag-generation mechanism for recording cell-tissue interactions. c, Galactose oxidase (GAO) can efficiently catalyze the oxidation of cell surface-exposed galactose (Gal) or *N*-acetylgalactosamine (GalNAc) to generate the bio-orthogonal aldehyde tag in situ.

properties of galactose oxidase (GAO). GAO can catalyze the oxidation of galactose/*N*-acetylgalactosamine (Gal/GalNAc, widely expressed in mammalian cells)[4c] at the end of cell surface glycan chains by O_2, forming a bio-orthogonal aldehyde group at the C6 position (Scheme 1c).[6] When GAO is mounted on a bait cell, the aldehyde groups produced on the prey cell during cell interactions can be used as minimum-sized reporters. This is also the first report on the use of GAO for cellular interaction recording.

We first demonstrated the feasibility of *GalTag* and its ability to monitor various interactions using the models of cancer/normal cell binding to endothelial cells (ECs). We then explored the application of *GalTag* in different in vitro biological scenarios: obtaining information about cellular interaction networks in a complex triple-cell system simulating a "tumor-complicated diabetes model"; tracking the dynamic EC-leukocyte interactions upon treatment of oxidatively stressed ECs with different metabolic salvage protocols; and assessing the targeting ability of engineered cells. In particular, we advanced the ability to collect information about interactions from *between individual cells* to *in biological solid regions*, allowing the exploration of granulosa cell-oocyte interactions across the zona pellucida. Finally, we recorded the Bacillus Calmette-Guérin (BCG) invasion into the bladder urothelium of living mice using *GalTag*, providing the footprint information of in vivo cell-solid tissue interaction and demonstrating the powerful and versatile application capabilities of *GalTag*.

Results and Discussion

GalTag and its Transcellular Tagging Performance

The kinetic characteristics of GAO are well-suited for recording cellular interactions. In the absence of cellular interactions, the high K_m for Gal (167.5 mM, Figure S1)[7] ensures a low tagging background.[4c] When intercellular interactions occur, GAO is saturated by Gal/GalNAc on the prey surface. The reaction rate is determined by k_{cat} (1741 s^{-1}, Figure S1),[7] which is the largest in current contact-dependent reporting systems (e.g., 13.2 s^{-1} in EXCELL[4b] and 7.4 s^{-1} in FucoID[4c]), thus guaranteeing maximum catalytic labeling efficiency.

We first verified the specificity of GAO towards exposed Gal/GalNAc (Figure S2) and the oxidation capability on various cell surfaces (Figure S3). To mount GAO on bait cells, we chose *N*-acetylneuraminic acid (NeuAc) as the anchor point. An aldehyde group can be easily introduced at the C7 position of NeuAc by mild periodate oxidation,[8] allowing coupling with hydrazide-modified GAO (GAO_{HZ}) (Figure 1a). GAO_{HZ} was prepared by linking the carboxyl groups of GAO with adipic dihydrazide (ADH) (Figure S4). With approximately 6 ADHs attached to each GAO, GAO_{HZ} exhibited a K_m value of 201.6 mM for Gal and a k_{cat} of 1096 s^{-1} (Figure S4). It maintained 60 % and 80 % (Figure 1b) enzymatic activity against Gal/GalNAc in solution and on live human umbilical vein endothelial cells (HUVECs, high glucose (HG) cultured), respectively.

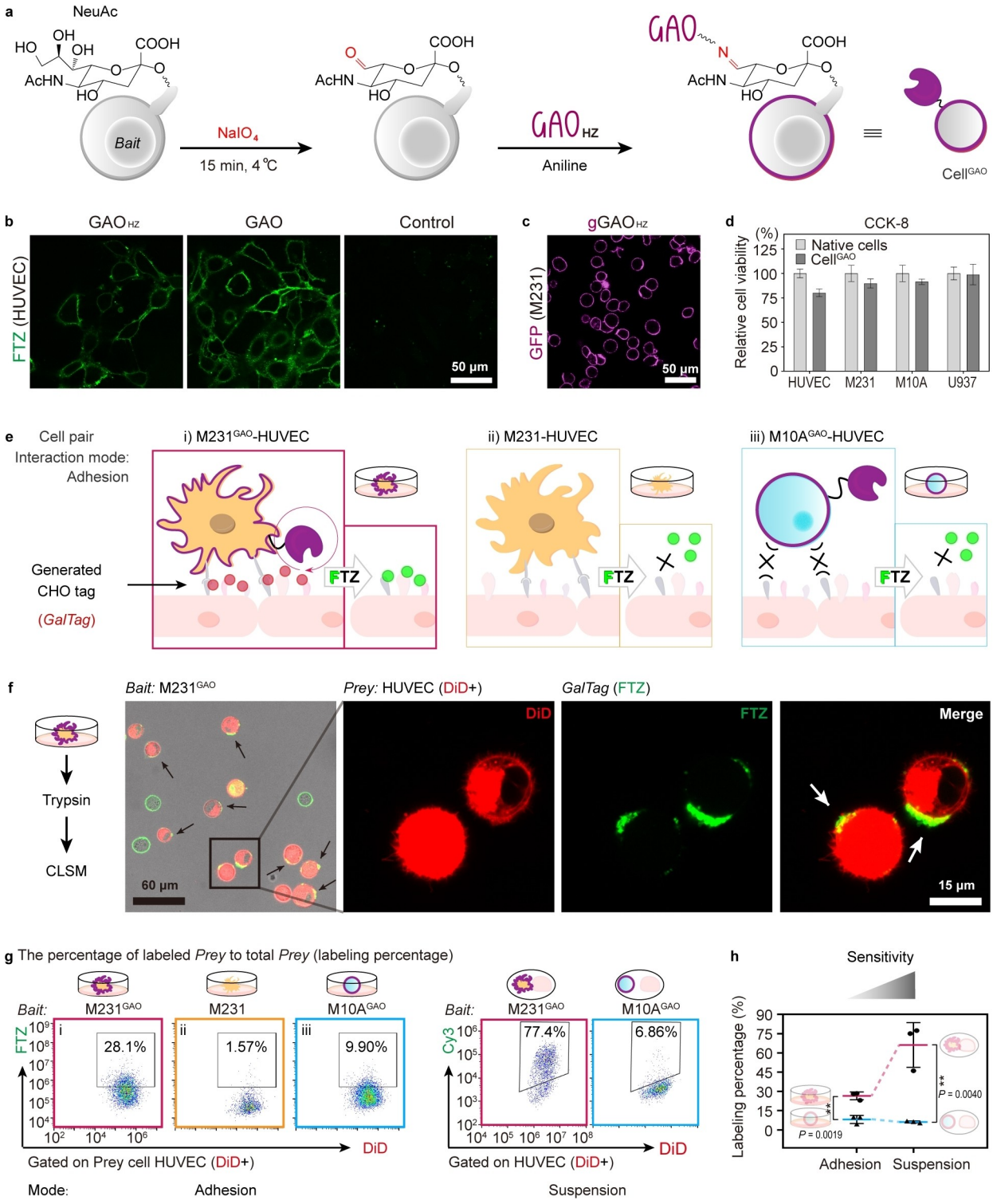

Figure 1. Probe design and *GalTag* performance. a, Schematic of the installation process of GAO_{HZ} on bait cells. b, Representative confocal laser scanning microscopy (CLSM) images of human umbilical vein endothelial cells (HUVECs) undergoing GAO_{HZ} (or GAO) oxidation and fluorescein-5-thiosemicarbazide (FTZ) staining. $n=3$ independent experiments. c, CLSM verification of the mounting of GAO_{HZ} on MDA-MB-231 (M231) cells using 2.9 μM green fluorescent protein (GFP)-conjugated GAO_{HZ} ($gGAO_{HZ}$). $n=3$ independent experiments. d, CCK-8 analysis of cell viability of GAO_{HZ}-conjugated cells ($Cell^{GAO}$). Data are shown as the mean ± SD, $n=3$. e, Scheme showing the in situ tag generation (*GalTag*, red sphere) induced by the interaction between GAO-mounted, suspended bait cells ($M231^{GAO}$, i) and adherent prey cells (HUVECs). Two control groups: M231 cells without GAO mounting as bait (ii), and $M10A^{GAO}$ as bait (iii). The generated CHO tag is further stained by FTZ (green sphere) for CLSM or flow cytometric (FCM) detection. f, Representative CLSM images of $M231^{GAO}$ (bait) and HUVECs (prey) undergoing *Gal-Tagging*, FTZ staining and trypsin treatment. Images for the control cell pairs are in Figure S10. $n=3$ independent experiments. g, FCM analysis of the *GalTag* labeling percentage of adhesion (left) and suspension (right) modes. h, Comparison of the two modes. Data are shown as the mean ± SD, $n=3$. *P* value was determined by unpaired two-tailed *t*-tests, $^{**}P \leq 0.01$.

We produced green fluorescent protein (GFP)-modified GAO (gGAO) and hydrazide-modified gGAO ($gGAO_{HZ}$) (Figure S5) to demonstrate the mounting of GAO_{HZ} on cell surfaces (Figures 1c, S6 and S7). GAO_{HZ}-anchored cells ($Cell^{GAO}$) showed viability comparable to natural cells (Figure 1d). The anchored amount of GAO_{HZ} can be regulated by varying the concentration of GAO_{HZ} (Figure S8).

To demonstrate the feasibility of transcellular *Gal-Tagging*, we adopted a cell adhesion model commonly used to study breast cancer metastasis: suspended human epithelial breast cancer cells MDA-MB-231 (M231) + adhered HUVECs[9] (i and ii of Figure 1e). HUVECs (prey) were DiD-stained unless otherwise stated. After incubating 1:1 mixed $M231^{GAO}$ and HUVECs on a shaker for 30 min (i of Figure 1e), we collected HUVECs for fluorescein-5-thiosemicarbazide (FTZ) staining[10] and imaging (Figure 1f). Crescent-shaped FTZ fluorescence emerged on the surface of HUVECs (red), completely different from the ring-shaped fluorescence observed from the cells treated with freely-diffused GAO (Figure S9). In contrast, incubation of GAO_{HZ}-free M231 cells and HUVECs (Control, ii of Figure 1e) resulted in background FTZ fluorescence (Figure S10a). These results confirm the transcellular oxidation by mounted GAO when the two cells are in contact. The labeling percentage of HUVECs recorded by flow cytometric (FCM) (Figures 1g, left (i,ii), S11 and S12) were in good agreement with the imaging results. The feasibility of transcellular tagging was further verified by exchanging the adhesion/suspension status of the two cell lines as well as the GAO-anchored objects, and consistent results were obtained (Figure S13).

To demonstrate that the labeling percentage can reflect the trend of cell-cell interactions, we introduced a control cell pair: $M10A^{GAO}$ (bait, human non-tumorigenic epithelial cells MCF-10A) + HUVECs (prey) (iii of Figure 1e). The labeling percentage was significantly lower than that for $M231^{GAO}$-HUVEC pair (Figures 1g (i, iii), S10b and S12). We firstly excluded the influence of generated hydrogen peroxide on labeling performance (Figure S14). Given the approximate GAO quantities on M231 and M10A cells (Figure S8), the decreased labeling percentage indicated a weaker interaction between M10A and HUVECs, which was consistent with conventional adhesion assays (Figure S15a). These suggest that *Gal-Tagging* is driven by cell-to-cell interactions rather than the affinity of GAO towards its glycan substrates, and *GalTag* is an effective tool for monitoring difference of intercellular interactions.

GalTag can also be applied in suspension cell mode (Figures 1g (right), S16a and S17), showing a greater differentiation between different interactions (Figure 1h). This may be due to the fact that by this mode, interactions occur more easily, increasing the sensitivity of *GalTag*.

We further investigated the applicability scope of *GalTag* to quantitatively compare different interactions by varying the anchoring amount of GAO_{HZ} on bait cells or the glycan substrate level on prey cells. When the GAO anchoring amount was reduced to 11.5 %, the prey labeling percentage remained essentially unchanged (Figure S18a,b). Limited by the specificity and efficiency of the glycosidases, the glycan substrate level was only reduced to 50 %, where the prey labeling percentage remained unchanged (Figure S18c–f).

Revelation of the Interaction Network

We next used *GalTag* to obtain information about interactions in more complex triple-cell systems. According to population investigations, individuals with diabetes show increased cancer risk.[11] The mechanisms behind it remain unclear, as cancer is usually the ultimate diagnosis of long-term metabolic diseases.[12] However, few studies have incorporated tumor cells into diabetic cell models. We are interested in the cell interaction network that exists in tumor-complicated diabetes.

We constructed a simulation model: human leukocytes U937 (U937) + ECs (HUVECs) + tumor cells (M231). HUVECs and M231 cells have similar Gal/GalNAc levels (Figure S3). *Gal-Tagging* of the dual-cell systems (1:1) $U937^{GAO}$ + HUVECs and $U937^{GAO}$ + M231 (Figure S19) showed that the former had a stronger interaction trend than the latter (Figure 2a), which was consistent with the adhesion experiment results (Figure S15b).

Gal-Tagging in the triple-cell system ($U937^{GAO}$, DiD-stained HUVECs, DiO-stained M231; 2:1:1) resulted in consistent interaction trends (Figures 2b–d and S16b). While the difference between the two interactions was amplified due to the competition between HUVECs and M231 (Figure 2e). These data provide a new perspective for understanding the role of aberrant glucose metabolism in promoting tumor migration: in diabetic settings, leukocytes interact strongly with ECs rather than tumor cells, potentially disrupting EC integrity and creating a more permissive pathway for tumor cell infiltration and metastasis.

Monitoring of the Dynamics of Cellular Interactions

We next investigated whether *GalTag* can respond to changes in interactions caused by alterations (state or function) in prey or bait cells, respectively. Two primary therapeutic strategies for "metabolic syndrome associated cancer" involve altering cellular metabolic environment and targeting the tumor. Using $U937^{GAO}$ cells as bait, we tracked the changes in the interactions between U937 and HUVECs under metabolic intervention and the changes in the targeting ability of $U937^{GAO}$ after installation of a targeting module.

Diabetics have chronically elevated blood glucose (i.e., HG) levels, resulting in inflammatory oxidative stress in the vascular endothelium.[13] Insulin (In) or restoration to the normal glucose environment helps to rescue the endothelial regulatory pathway that is impaired by HG. We simulated this situation in vitro: After prolonged exposure to HG, HUVECs were salvaged in three ways (Figure S20): 1) insulin (HG + In); 2) normal glucose (NG); and 3) NG + In (Figure 3a). *GalTag* was used to monitor changes in interaction intensity. The three groups showed a similar

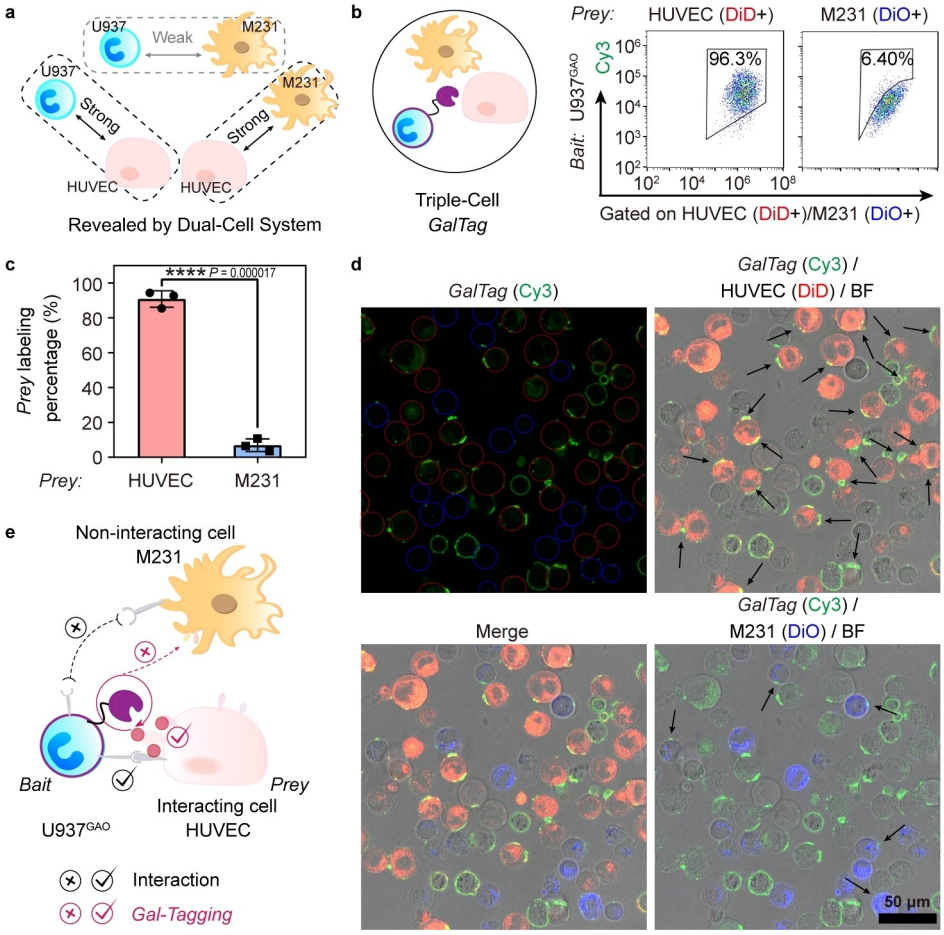

Figure 2. Revelation of the interaction network in the simulated tumor-complicated diabetes model with *GalTag*. a, Summary of the interaction strength obtained with the dual-cell *GalTag* (Details in Figures 1g and S19). b–c, FCM analysis of the labeling percentage of HUVECs and M231 by U937^{GAO} in a triple-cell competition model. Data are shown as the mean ± SD, $n = 3$. *P* value was determined by unpaired two-tailed *t*-tests; ****$P \leq 0.0001$. d, Representative CLSM images of b. BF, bright field. The HUVECs and M231 are indicated by red and blue circles in the upper left image. $n = 3$ independent experiments. e, Schematic of using *GalTag* to simultaneously record the U937^{GAO}-HUVEC and U937^{GAO}-M231 interactions.

degree of decrease in labeling percentage (Figures 3b and S21a), while maintaining basically unchanged Gal/GalNAc level (Figure S21b). This indicates a diminished adhesion capacity of HUVECs, as evidenced by the reduction in the expression of intercellular cell adhesion molecule-1 (ICAM-1)[14] (Figure 3c). However, the adhesion assay hardly reported such subtle changes (Figure S15c). These results provide insights into the relationship between cellular oxidative stress state and adhesion behaviors. Since the inherent interaction between U937 and M231 cells was weak (Figure S19), to enhance the interaction between U937 and M231 for targeted therapy, we conferred the M231-targeting ability to U937^{GAO} by co-mounting an aptamer that specifically binds M231 cells[15] (Figures 3d and S22). The labeling percentage on M231 by U937$^{AS1411+GAO}$ was higher than that by U937^{GAO} (Figures 3e,f and S23). The above two experiments together demonstrate the capability of *GalTag* to reflect changes in prey or bait cells and thus in the interactions.

Recording of the Traverse of Granulosa Cells through the Zona Pellucida of Oocytes

Next, we investigated whether *GalTag* could be used in biological solid regions, using granulosa cell (GC)-oocyte (Oo) interaction system as a model. During follicle development, GCs enclose Oo and directly contact with the zona pellucida (ZP, a 2–25 μm thick glycoprotein solid layer)[16] of Oo. GCs extend transzonal projections (TZPs) in ZP for information exchange and material transfer with Oo.[17] This interaction is essential to promote oocyte maturation and development. Understanding GC–Oo interaction can provide insight about factors that lead to infertility and miscarriages.

We extracted the cumulus-oocyte complexes from female ICR mice, and separated Oo and GCs (Figure 4a). Since oocytes are very limited in quantity and sensitive to environment change, we designated them as prey cells. We first confirmed the distribution of glycan substrates for GAO throughout the ZP of Oo (Figures 4b and S24). We

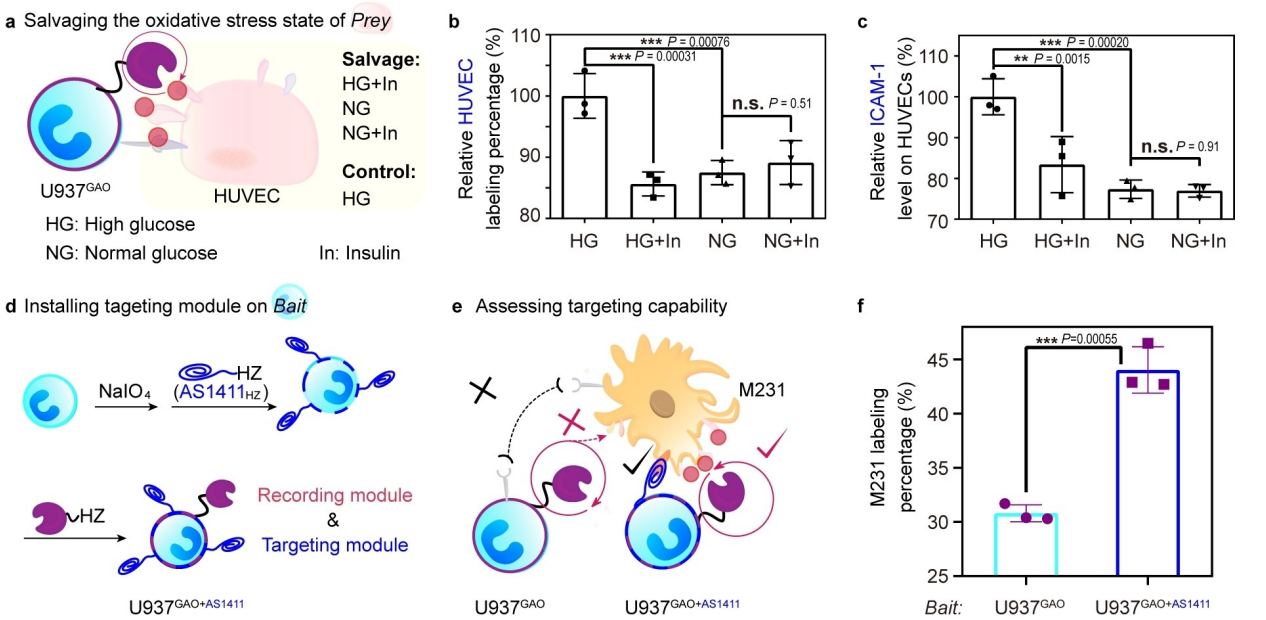

Figure 3. Monitoring of the dynamics of cellular interactions using *GalTag*. a, Schematic of monitoring the U937^{GAO}-HUVEC interaction in response to different metabolic salvage treatments. b, FCM analysis of the labeling percentage of HUVECs in different groups (relative to HG group). c, FCM analysis of the surface intercellular cell adhesion molecule-1 (ICAM-1) expression levels of HUVECs in different groups (relative to HG group). Data in (b,c) are shown as the mean ± SD, $n = 3$. *P* value was determined by an ordinary One-Way ANOVA test. $^{**}P \leq 0.01$, $^{***}P \leq 0.001$, and $P > 0.05$ was considered not significant (n.s.). d, Schematic of the installation of the targeting (AS1411$_{HZ}$) and recording (GAO$_{HZ}$) modules on bait cells (U937). e, Scheme showing the principle of using *GalTag* to assess the targeting capability of U937 to M231 before and after the installation of the targeting module (AS1411). f, FCM assessment of the labeling percentage of prey (M231) after incubation with bait^{GAO} cells (U937) with/without AS1411$_{HZ}$ mounting. Data are shown as the mean ± SD, $n = 3$. P value was determined by unpaired two-tailed t-test; $^{***}P \leq 0.001$.

then produced GC^{GAO} (or GC^{gGAO}) as bait (Figure S25) and blocked their residual aldehyde groups (Figure S26a,b). The interaction of GC^{GAO} and Oo initiated *Gal-Tagging*, generating *GalTag* that can be visualized by hydrazide-modified fluorescent molecule (F-HZ) staining (Figure 4a).

2-dimensional and 3-dimensional reconstruction images (Figures 4c, S26c,d, and Supplementary Video 1) showed punctated *GalTag* signals throughout ZP. This pattern was divergent from that for Oo treated with freely-diffused GAO (Figures 4b and S24). To localize *GalTag* and explore the mechanism of GC–Oo interaction, we stained actin of Oo after performing *Gal-Tagging* (actin is the main component of TZPs).[17b] The fluorescence signals of actin consisted of filopodia of GCs (TZPs) penetrating ZP, and the oocyte plasma membrane, i.e., oolemma (bright circle, Figure S24). *GalTag* signals in ZP were mostly distributed near TZPs (Figure 4c and Supplementary Video 2), and also presented on oolemma (Figure 4c,d).

We confirmed the attachment of GCs to oolemma via TZPs in ZP (Figure S27); the presence of small amounts of gGAO in ZP (Figure S28a) and on oolemma (Figure S28b) after *Gal-Tagging*; and the inability of freely-diffused GAO to label oolemma (Figure S24). These collectively suggest that GC^{GAO} utilizes TZPs in ZP to enable the GAO on the GCs to perform oxidation on oolemma.

This is the first successful attempt to study GC–Oo interaction using a proximity labeling technology and highlights the ability of *GalTag* to record bait cell footprints in biological solid regions. Our finding that ZP is tolerant to cargoes carried by GCs to enter inside provides new insights into understanding and exploiting the selective protective role of ZP during oocyte growth.

In Vivo Recording of Bait Footprints in Solid Tissues

Finally, we constructed an in vivo model to investigate the feasibility of using *GalTag* to record bait footprints in solid tissues. Postoperational intravesical instillation of BCG is the standard treatment for bladder cancer.[18] However, the antitumor effects of BCG are unclear[18,19] and the interactions involved need to be elucidated. We verified the glycan substrate abundance for GAO in bladders of C57BL/6 mice (Figure S29), successfully installed GAO on BCG (Figure S30a–c), and chose EGFP-transfected BCG (gBCG, strain: rBCG-S.EGFP, green light) as bait for in vivo experiments.

We instilled gBCG^{GAO} (*GalTag* group) or gBCG (control group) into mouse bladders in the presence of F-HZ (IR783$_{HZ}$) (Figure 5a) and incubated for 2 h prior to imaging. Compared with the control group, the bladders of the *GalTag* group showed stronger in vivo and ex vivo fluorescence (Figures 5b and S31a; and Figure S30d excluded the interference from fluorescence adsorption), and their cell suspensions had a higher level of *GalTag* labeling percentage (Figures 5c and S31b), collectively demonstrating the feasibility of using BCG as bait for in vivo *Gal-Tagging*.

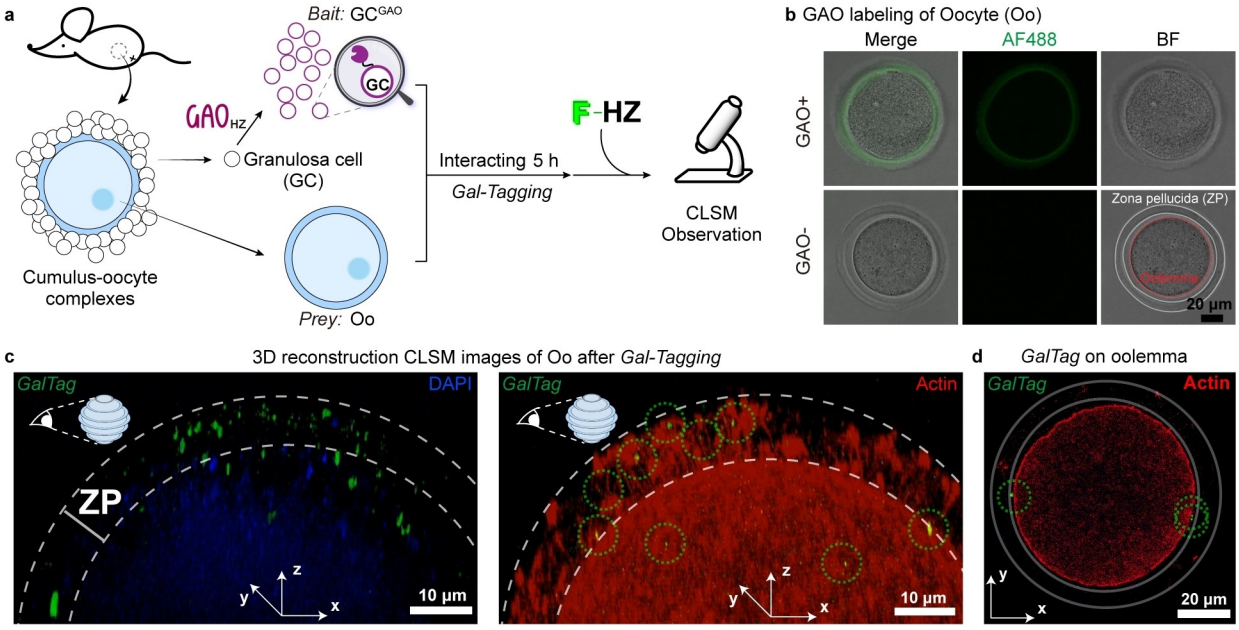

Figure 4. In vitro recording of granulosa cell-oocyte trans-zona pellucida interaction using *GalTag*. a, Schematic of the procedure of preparation of GAO-mounted granulosa cells (GC^{GAO}, bait) and oocytes (Oo, prey) for *Gal-Tagging* and fluorescence staining. b, Representative CLSM images showing the labeling pattern of Oo by freely-diffused GAO and $AF488_{HZ}$ (green). The region between the two white circles shows the zona pellucida (ZP). Red indicates the oolemma. Fluorescence signals emerged only in ZP. $n=3$ independent experiments. c, Representative 2-dimensional perspective view of the 3-dimensional reconstruction CLSM images of Oo after incubation with GC^{GAO} and subsequent $AF488_{HZ}$ staining. Green ($AF488_{HZ}$) indicates *GalTag*. Blue (DAPI) indicates nucleic acids in Oo. Red (phalloidin-iFluor 594) indicates actin. The region between the two dashed lines indicates the position of ZP at the largest diameter in the xz plane perpendicular to y-axis. Within ZP, actin indicates transzonal projections (TZPs), while within the inner dashed line, actin indicates oolemma. The *GalTag* signals (indicated with green dotted circles) are located in the ZP of Oo (close to the TZPs) or on the oolemma. $n=4$ independent experiments. d, Representative 2-dimensional CLSM image of Oo after *Gal-Tagging* (by GC^{GAO}) and $AF488_{HZ}$ staining. The *GalTag* (green) were distributed on the oolemma (indicated by green dotted circles). Red indicates actin. Within the ZP (between the two grey circles) of Oo, actin indicates the TZPs, while within the inner grey circle, the bright red circle indicates the oolemma. $n=4$ independent experiments.

Next, we scrutinized the footprints of $gBCG^{GAO}$ in bladder frozen sections (Figures 5d–e and S32). Hydrazide-modified AF594 ($AF594_{HZ}$) was instilled instead of $IR783_{HZ}$ together with $gBCG^{GAO}$ to directly stain the generated aldehyde groups for imaging. This mode simulates the "tag-transfer mechanism" to some extent. $gBCG^{GAO}$ showed green or yellow (due to adsorption of $AF594_{HZ}$ (red)) pseudocolor. The red signals, which were not spatially superimposed on the green signals, corresponded to *GalTag* signals.

In normal bladder sections (Figure 5d), the distribution of $gBCG^{GAO}$ at mouse sacrifice moment was in the urothelium (e.g., regions i and ii of d). *GalTag* signal showed a punctuated or linear pattern along the bladder urothelium. While, in the sections of MB49 in situ bladder cancer mice (Figure 5e), the distribution of $gBCG^{GAO}$ was in the urothelium (e.g., regions i and ii of e) and tumor cavity regions (which might be connected to the bladder lumen) (e.g., iv of e). The *GalTag* signals were distributed along the surface of the urothelium (e.g., regions i and ii of e), tumor-cavity interfaces (e.g., iv of e), and to a lesser extent on the surface of the tumor tissue on the opposite side of the urothelium (e.g., iii of e). Due to the absence of GAO on the BCG in the control group, only weak red signals could be observed, which were almost co-localized with (adsorbed on) the green signals.

The differences between the normal and cancer groups are quite interesting. In normal bladders, the *GalTag* fluorescence signal was primarily located in the mucus layer, detached from the urothelium surface, and did not overlap with the green fluorescence signal of gBCG. We speculate that the intact mucus layer allows the invasion of $gBCG^{GAO}$ into the urothelium while blocking $AF594_{HZ}$ from penetrating. In the bladder cancer model, the *GalTag* signals, confined to the outermost surface of the urothelium, suggest that F-HZ can cross the impaired mucus barrier but can not easily penetrate the outermost surface of the urothelium ($AF594_{HZ}$ in Figure 5e or $AF647_{HZ}$ in Figure S33). As we increased the number of instillation rounds, both the $gBCG^{GAO}$ and *GalTag* signals occurred deeper in the tissue, but the *GalTag* signals still lagged behind $gBCG^{GAO}$ (Figure S33).

These data first substantiate our design that the *GalTag* technology can in vivo record the "footprints of bait" rather than the "location of bait". At the same time, the results demonstrate the tag-distribution-dependent issue of "tag-transfer mechanism": due to the limited diffusion capacity of tag molecules in solid tissues, only part of the footprints can be recorded by the in vivo staining mode.

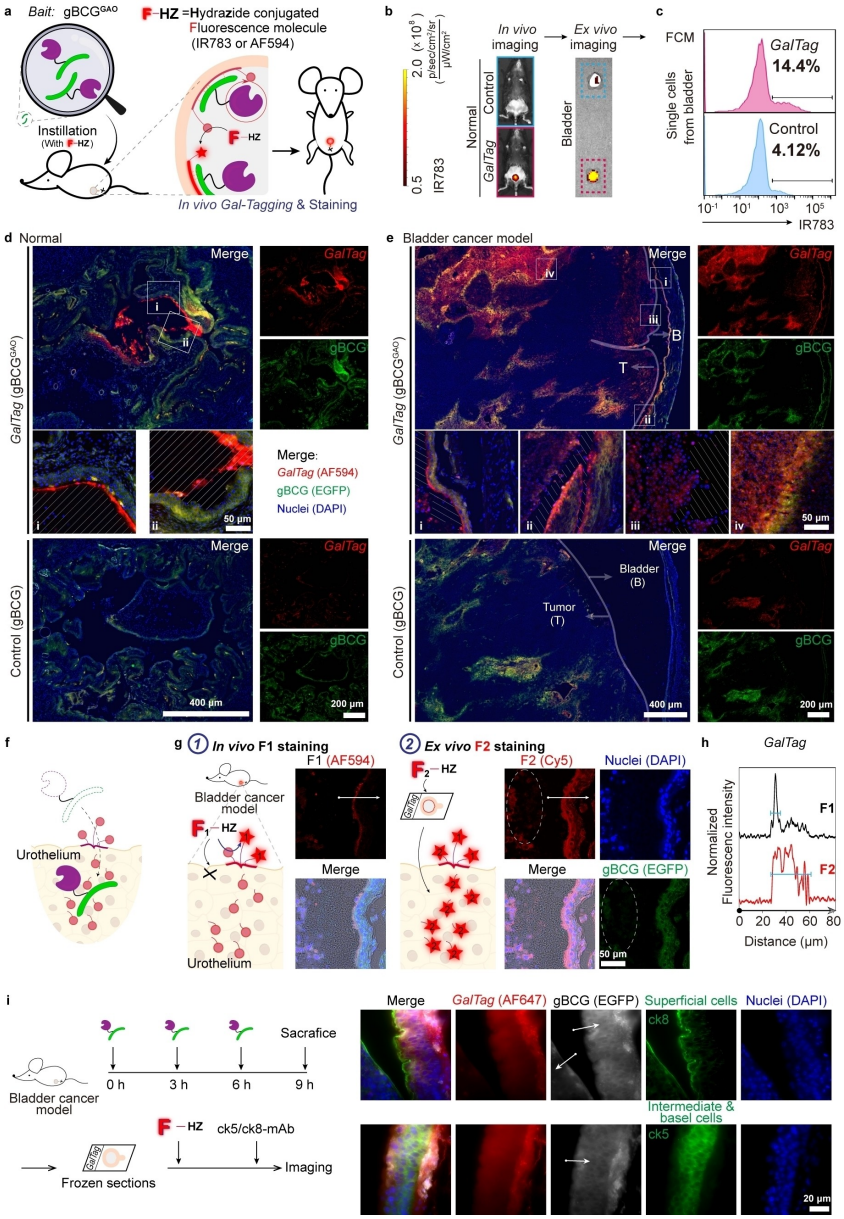

Figure 5. In vivo recording of BCG footprints in bladders with *GalTag*. a, Schematic of in vivo *Gal-Tagging* & staining. gBCG^{GAO}, EGFP-BCG^{GAO}. b, Representative in vivo fluorescence images of C57BL/6 mice (normal) and ex vivo fluorescence images of bladders after performing in vivo *Gal-Tagging* & staining. c, FCM analysis of IR783 fluorescence of single cells obtained from the bladders in b. $n=3$ independent experiments. d-e, Representative fluorescence images of frozen bladder sections from normal (d) and MB49 in situ bladder cancer model mice (e) after in vivo *Gal-Tagging* and AF594$_{HZ}$ staining. T, tumor; B, bladder. Sections treated with gBCG (without GAO anchored) were used as controls. In both groups, the largest images show merged fluorescence signals: red represents AF594$_{HZ}$; green (EGFP) indicates the position of gBCG^{GAO} (Figure S37 shows the adhesion pattern of gBCG on living L929 cells); blue indicates cell nuclei. Scale bar: 400 μm. The boxed regions indicate the positions of magnified images shown in the middle. The regions (i~ii) in d correspond to the mucus-coated urothelium. The regions (i~iii) in e correspond to the surface of urothelium or tumor; region iv is the margin of one tumor cavity. Italic lines indicate regions of the bladder lumen where gBCG^{GAO} and AF594$_{HZ}$ were instilled. Scale bar: 50 μm. The single fluorescence channel images are shown on the right of the merged images. Scale bar: 200 μm. $n=3$ independent experiments. f, Schematic showing the generation of *GalTag* (red sphere) not only on the surface of the urothelium but also inside the tissue, allowing the recording of the complete footprints of gBCG^{GAO}. g, After performing in vivo *Gal-tagging* & staining (AF594$_{HZ}$, F1), bladder tissue sections from MB49 cancer model mice were obtained and subjected to CLSM imaging, followed by the second round of fluorescence staining with Cy5-BSA$_{HZ}$ (F2; see Figure S36 for the control experiment) and CLSM imaging. Red indicates the fluorescently-stained *GalTag*. Scale bar: 50 μm. $n=6$ independent experiments. h, Normalized fluorescence intensity (FI) along the arrows drawn in the red channel images of g. i, After three rounds of BCG^{GAO} instillation and in vivo *Gal-Tagging*, bladder tissue sections from MB49 cancer model mice were obtained and subjected to AF647$_{HZ}$ staining, immunohistochemical staining (cytokeratin 5 (ck5) and cytokeratin 8 (ck8)), and fluorescence imaging. Grey (EGFP) indicates the position of gBCG^{GAO}; green indicates ck5 or ck8. Ck5 (low) and ck8 (high) indicate bladder superficial cells, ck5 (low) and ck8 (moderate) indicate intermediate cells, ck5 (high) and ck8 (low) indicate basal cells, and the regions under the basal cells that cannot be labeled by either antibody are lamina propria. The arrows drawn in the grey channel images show the direction of BCG invasion. $n=3$ independent experiments.

We also replaced GAO with horseradish peroxidase (HRP) and constructed a transcellular labeling system based on HRP-catalyzed phenol radical labeling to report the gBCG-bladder interactions (Figures S34 and S35). With co-instillation of hydrogen peroxide and fluorescence-modified tyramide, only a few labeling sites were observed, presumably because gBCG and the substrates could not move synchronously.

In particular, the aldehyde tags generated by BCG^{GAO} inside the tissue (Figure 5f) can be lit up ex vivo to give complete bait footprints. To demonstrate this, we performed ex vivo staining on frozen sections from the mice undergoing in vivo *Gal-Tagging* & staining. Unlike in vivo fluorescence staining (which produced a *GalTag* signal superficial to the surface of the urothelium), ex vivo staining produced a labeled band tens of microns deep into the bladder tissue (red, Figures 5g,h and S36). The red signals represent the *complete* footprints of $gBCG^{GAO}$. When increasing the number of instillation rounds, the depth of *GalTag* signal reached the final position of $gBCG^{GAO}$, crossing the basal cell layer and extending into the lamina propria where few cells existed (Figure 5i).

For one round of instillation, the distribution difference between *GalTag* and gBCG (Figure 5e) suggests that gBCG actively interacts with various accessible interfaces during the initial stage of instillation, but is ultimately enriched in the urothelium and cavities within the tumor rather than on the tumor surface. The regions marked with circles in Figure 5g further suggest that BCG may leave the tumor tissue after interacting with the tumor. This is the first time that the BCG invasion footprints during the instillation therapy have been revealed, providing a valuable scientific perspective to elucidate the anti-tumor mechanism of BCG. These data collectively demonstrate the application of *GalTag* technology in cell-solid tissue interaction scenarios.

Conclusion

In summary, we have developed a GAO-based *GalTag* technology to track physical cell contacts by transcellular oxidation of Gal/GalNAc adjacent to cell-cell interaction sites to generate aldehyde groups. The technology is characterized by the in situ generation of a bio-orthogonal tag without the need for exogenous reactive tags and in a contact-dependent, enzyme-catalyzed manner, resulting in extremely high fidelity and sensitivity. Glycoproteins comprise 50 % of the human proteome. Glycans are widely expressed on the surface of mammalian cells, bacteria and fungi.[20] Therefore, GAO_{HZ} can be mounted on a wide range of cell surface to detect different types of contacts.

Diverging from current proximity labeling methods primarily applicable to interactions between single suspension cells, *GalTag* is unique in that it allows the study of cellular interactions occuring in biological solid regions, as confirmed in two scenarios: in vitro granulosa cell-oocyte interaction across the zona pellucida (Figure 4c,d) and in vivo BCG-bladder interaction (Figure 5d–i). Bait can "*tag as they go around*", which is neither dependent on the addition of tags nor affected by the tag diffusion properties. This fundamentally addresses the challenge of in situ cell footprinting in solid tissues.

In the future, "temporal control" of *GalTag* can be achieved by installing a photosensitive switch near the active site of GAO to report interactions at specific time points/phases. Besides, combined with proteomics technologies, *GalTag* can reveal information at the molecular level during cellular interactions. Moreover, by attaching GAO to a specific protein on the cell surface, we can obtain information on the interactions involving the protein of interest in biological processes.

In conclusion, *GalTag*, as the first technology to generate tags in situ to record cellular interactions, demonstrates excellent capabilities and application potential in various in vitro and in vivo scenarios. We strongly believe that *GalTag* will be a powerful tool to gain insights into tissue formation, neurotransmission, gamete development, microbial invasion and immune processes, and will contribute to the development of cell-based therapies and assisted reproductive technologies.

Supporting Information

The authors have cited additional references within the Supporting Information.[21–23]

Acknowledgements

We gratefully acknowledge support from the National Natural Science Foundation of China (22274073, 21974067), Fundamental Research Funds for the Central Universities (020514380309, 021414380502, 2022300324), and the State Key Laboratory of Analytical Chemistry for Life Science (5431ZZXM2305, 5431ZZXM2204).

Conflict of Interest

The authors declare no conflict of interest.

Data Availability Statement

The data that support the findings of this study are available from the corresponding author upon reasonable request.

Keywords: Bacillus Calmette-Guérin · Bio-orthogonal labeling · Cell interaction recording · Endogenous substrate · Galactose oxidase

[1] a) M. Furuya, J. Kikuta, S. Fujimori, S. Seno, H. Maeda, M. Shirazaki, M. Uenaka, H. Mizuno, Y. Iwamoto, A. Morimoto, K. Hashimoto, T. Ito, Y. Isogai, M. Kashii, T. Kaito, S. Ohba, U. I. Chung, A. C. Lichtler, K. Kikuchi, H. Matsuda, H. Yoshikawa, M. Ishii, *Nat. Commun.* **2018**, *9*, 300; b) B. Belardi,

S. Son, J. H. Felce, M. L. Dustin, D. A. Fletcher, *Nat. Rev. Mol. Cell Biol.* **2020**, *21*, 750–764; c) B. N. Manz, J. T. Groves, *Nat. Rev. Mol. Cell Biol.* **2010**, *11*, 342–352; d) M. Feng, W. Jiang, B. Y. S. Kim, C. C. Zhang, Y. X. Fu, I. L. Weissman, *Nat. Rev. Cancer* **2019**, *19*, 568–586; e) S. Qiu, Z. Zhao, M. Wu, Q. Xue, Y. Yang, S. Ouyang, W. Li, L. Zhong, W. Wang, R. Yang, P. Wu, J. P. Li, *Sci. Adv.* **2022**, *8*, eadd2337.

[2] a) T. J. Bechtel, T. Reyes-Robles, O. O. Fadeyi, R. C. Oslund, *Nat. Chem. Biol.* **2021**, *17*, 641–652; b) Y. Liu, Y. Ge, R. Zeng, W. S. C. Ngai, X. Fan, P. R. Chen, *CCS Chemistry* **2023**, *5*, 802–813.

[3] a) R. C. Oslund, T. Reyes-Robles, C. H. White, J. H. Tomlinson, K. A. Crotty, E. P. Bowman, D. Chang, V. M. Peterson, L. Li, S. Frutos, M. Vila-Perelló, D. Vlerick, K. Cromie, D. H. Perlman, S. Ingale, S. D. O. Hara, L. R. Roberts, G. Piizzi, E. C. Hett, D. J. Hazuda, O. O. Fadeyi, *Nat. Chem. Biol.* **2022**, *18*, 850–858; b) H. Liu, H. Luo, Q. Xue, S. Qin, S. Qiu, S. Liu, J. Lin, J. P. Li, P. R. Chen, *J. Am. Chem. Soc.* **2022**, *144*, 5517–5526; c) K. H. Loh, P. S. Stawski, A. S. Draycott, N. D. Udeshi, E. K. Lehrman, D. K. Wilton, T. Svinkina, T. J. Deerinck, M. H. Ellisman, B. Stevens, S. A. Carr, A. Y. Ting, *Cell* **2016**, *166*, 1295–1307.e1221; d) J. B. Geri, J. V. Oakley, T. Reyes-Robles, T. Wang, S. J. McCarver, C. H. White, F. P. Rodriguez-Rivera, D. L. Parker Jr., E. C. Hett, O. O. Fadeyi, R. C. Oslund, D. W. C. MacMillan, *Science* **2020**, *367*, 1091–1097; e) X. Zhang, Q. Tang, J. Sun, Y. Guo, S. Zhang, S. Liang, P. Dai, X. Chen, *Sci. Adv.* **2023**, *9*, eadg6388; f) C. P. Seath, A. D. Trowbridge, T. W. Muir, D. W. C. MacMillan, *Chem. Soc. Rev.* **2021**, *50*, 2911–2926.

[4] a) G. Pasqual, A. Chudnovskiy, J. M. J. Tas, M. Agudelo, L. D. Schweitzer, A. Cui, N. Hacohen, G. D. Victora, *Nature* **2018**, *553*, 496–500; b) Y. Ge, L. Chen, S. Liu, J. Zhao, H. Zhang, P. R. Chen, *J. Am. Chem. Soc.* **2019**, *141*, 1833–1837; c) Z. Liu, J. P. Li, M. Chen, M. Wu, Y. Shi, W. Li, J. R. Teijaro, P. Wu, *Cell* **2020**, *183*, 1117–1133.e1119; d) Q. Liu, J. Zheng, W. Sun, Y. Huo, L. Zhang, P. Hao, H. Wang, M. Zhuang, *Nat. Methods* **2018**, *15*, 715–722.

[5] M. L. Dustin, T. A. Springer, *Nature* **1989**, *341*, 619–624.

[6] a) T. N. Ramya, E. Weerapana, B. F. Cravatt, J. C. Paulson, *Glycobiology* **2013**, *23*, 211–221; b) K. Parikka, E. Master, M. Tenkanen, *J. Mol. Catal. B* **2015**, *120*, 47–59.

[7] R. Lontie, *Copper Proteins and Copper Enzymes: Volume II, Vol. 2*, CRC press **2018**.

[8] Y. Zeng, T. N. Ramya, A. Dirksen, P. E. Dawson, J. C. Paulson, *Nat. Methods* **2009**, *6*, 207–209.

[9] Y. Connor, Y. Tekleab, S. Tekleab, S. Nandakumar, D. Bharat, S. Sengupta, *Sci. Rep.* **2019**, *9*, 8429.

[10] D. K. Kölmel, E. T. Kool, *Chem. Rev.* **2017**, *117*, 10358–10376.

[11] A. Goto, T. Yamaji, N. Sawada, Y. Momozawa, Y. Kamatani, M. Kubo, T. Shimazu, M. Inoue, M. Noda, S. Tsugane, M. Iwasaki, *Int. J. Cancer* **2020**, *146*, 712–719.

[12] V. Brower, *J. Natl. Cancer Inst.* **2012**, *104*, 1048–1050.

[13] a) S. Devaraj, M. R. Dasu, I. Jialal, *Expert Rev. Endocrinol. Metab.* **2010**, *5*, 19–28; b) F. Cosentino, M. Eto, P. De Paolis, B. van der Loo, M. Bachschmid, V. Ullrich, A. Kouroedov, C. Delli Gatti, H. Joch, M. Volpe, T. F. Lüscher, *Circulation* **2003**, *107*, 1017–1023; c) T. Yuan, T. Yang, H. Chen, D. Fu, Y. Hu, J. Wang, Q. Yuan, H. Yu, W. Xu, X. Xie, *Redox Biol.* **2019**, *20*, 247–260; d) Q. Yang, H. Yuan, M. Chen, J. Qu, H. Wang, B. Yu, J. Chen, S. Sun, X. Tang, W. Ren, *Life Sci.* **2018**, *198*, 56–64.

[14] a) T. A. Springer, *Nature* **1990**, *346*, 425–434; b) M. P. Bevilacqua, R. M. Nelson, G. Mannori, O. Cecconi, *Annu. Rev. Med.* **1994**, *45*, 361–378.

[15] a) C. R. Ireson, L. R. Kelland, *Mol. Cancer Ther.* **2006**, *5*, 2957–2962; b) J. E. Rosenberg, R. M. Bambury, E. M. Van Allen, H. A. Drabkin, P. N. Lara Jr., A. L. Harzstark, N. Wagle, R. A. Figlin, G. W. Smith, L. A. Garraway, T. Choueiri, F. Erlandsson, D. A. Laber, *Invest. New Drugs* **2014**, *32*, 178–187.

[16] P. M. Wassarman, *Annu. Rev. Biochem.* **1988**, *57*, 415–442.

[17] a) T. M. Plant, A. J. Zeleznik, *Knobil and Neill's physiology of reproduction*, Academic Press **2014**; b) S. El-Hayek, Q. Yang, L. Abbassi, G. FitzHarris, H. J. Clarke, *Curr. Biol.* **2018**, *28*, 1124–1131.e1123.

[18] C. Pettenati, M. A. Ingersoll, *Nat. Rev. Urol.* **2018**, *15*, 615–625.

[19] S. Jiang, G. Redelman-Sidi, *Cancers (Basel).* **2022**, *14*.

[20] J. Eichler, M. Koomey, *Trends Microbiol.* **2017**, *25*, 662–672.

[21] C. K. Stover, V. F. de la Cruz, T. R. Fuerst, J. E. Burlein, L. A. Benson, L. T. Bennett, G. P. Bansal, J. F. Young, M. H. Lee, G. F. Hatfull, et al., *Nature* **1991**, *351*, 456–460.

[22] Y. Luo, A. Szilvasi, X. Chen, W. C. DeWolf, M. A. O'Donnell, *Clin. Diagn. Lab. Immunol.* **1996**, *3*, 761–768.

[23] L. Kasman, C. Voelkel-Johnson, *J. Visualization* **2013**, e50181.

Manuscript received: April 15, 2024
Accepted manuscript online: May 3, 2024
Version of record online: ■■, ■■

Research Articles

Labeling Technologies

Y. Yao, R. Jia, C. Liu, H. Wang, T. Li, X. Zheng, T. Zhong, N. Feng, J. Sun, K. Li, R. Xie, L. Ding, C. Yan, L. Ding,* H. Ju e202407109

An *In-Situ*-Tag-Generation Proximity Labeling Technology for Recording Cellular Interactions

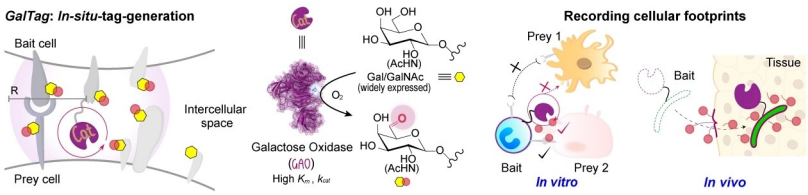

We propose an "in-situ-tag-generation mechanism" and develop the *GalTag* technology based on galactose oxidase (GAO) for recording cellular interactions. GAO mounted on bait cells can in situ generate bio-orthogonal aldehyde tags as interaction reporters on prey cells. *GalTag* is unique in that it eliminates the need to add tag molecules, resulting in the ability to record bait footprints in three-dimensional biological solid regions.